

Growth of p-doped 2D-MoS₂ on metal oxides from spatial atomic layer deposition

André Maas¹, Kissan Mistry², Stephan Sleziona¹, Abdullah H. Alshehri³, Hatameh Asgarimoghaddam², Kevin Musselman², Marika Schleberger¹

¹Universität Duisburg-Essen, Fakultät für Physik and CENIDE, Germany

²Department of Mechanical and Mechatronics Engineering, University of Waterloo, Canada

³Department of Mechanical Engineering, Prince Sattam bin Abdul Aziz University, Alkharj 11942, Saudi Arabia

Abstract. In this letter we report on the synthesis of monolayers of MoS₂ via chemical vapor deposition directly on thin films of Al₂O₃ grown by spatial atomic layer deposition. The synthesized monolayers are characterized by atomic force microscopy as well as confocal Raman and photoluminescence spectroscopies. Our data reveals that the morphology and properties of the 2D material differ strongly depending on its position on the substrate. Close to the material source, we find individual flakes with an edge length of several hundred microns exhibiting a tensile strain of 0.3%, n-doping on the order of $n_e=0.2 \times 10^{13} \text{ cm}^{-2}$, and a dominant trion contribution to the photoluminescence signal. In contrast to this, we identify a mm-sized region downstream, that is made up from densely packed, small MoS₂ crystallites with an edge length of several microns down to the nanometer regime and a coverage of more than 70%. This nano-crystalline layer shows a significantly reduced strain of only <0.02%, photoluminescence emission at an energy of 1.86 eV with a reduced trion contribution, and appears to be p-doped with a carrier density of $n_h=0.1 \times 10^{13} \text{ cm}^{-2}$. The unusual p-type doping achieved here in a standard CVD process without substitutional doping, post-processing, or the use of additional chemicals may prove useful for applications.

1. Introduction

In recent years there has been an increasing interest in 2D materials for high performance electronic and optoelectronic applications [1–3], including flexible devices [4–6] and field-effect transistors [7]. An important class of 2D materials is transition metal dichalcogenides (TMDC) with the chemical formula MX₂. The hexagonal structure is formed by a sheet of transition metal (M) atoms covalently bound in between two layers of chalcogen (X) atoms. Some TMDCs like molybdenum disulfide (MoS₂) have semiconductor properties like an indirect band gap in the near infrared. When their spatial extension is confined in one dimension this band gap becomes a direct band gap in the visible spectrum [8–10], making these materials even more attractive for (flexible) optoelectronics. This however requires the fabrication of heterostructures, i.e., the combination of the TMDC with at least one dielectric material. The current approach of layering MoS₂ on top of high- κ dielectrics utilizes growth via chemical vapour deposition (CVD) on selected substrates, typically SiO₂, and subsequent transfer onto the final dielectric materials. This process suffers from various limitations including the loss of structural integrity of the MoS₂ layer, no control over the doping, and contamination through residuals from the transfer process [11,12]. Growing the MoS₂ directly on top of the dielectric could overcome these severe limitations [7].

While this approach seems straightforward, it is still a challenge to obtain a continuous layer of MoS₂ using a common fabrication method such as CVD. The resulting monolayers are typically highly crystalline, but their lateral dimensions rarely exceed a few hundred microns [7,13]. Also, the large-scale fabrication of tailored dielectrics poses a major problem, in particular if the flexibility of the 2D material is to be maintained, requiring ultrathin dielectric films. To address both problems it has recently been tried to combine CVD growth of MoS₂ with the synthesis of the dielectric material via atomic layer deposition [7]. The resulting flakes were on average rather small (edge length of a few microns), could be processed into a working field-effect device and showed a PL signal at room temperature (RT). Atomic layer deposition (ALD) is already in use worldwide for the fabrication of microelectronics and can deposit nanolaminated stacks of films [14–16]. However, one of the biggest drawbacks of this technique is its low deposition rate and therefore it may not always be commercially viable considering the price and its limited throughput [17].

We therefore suggest to use the newly developed process of atmospheric-pressure spatial atomic layer deposition (AP-SALD) to overcome this drawback. This technique separates the precursor gases not temporally but spatially, making it a faster and more cost-effective way of creating a thin layer with sufficient control over the layer thickness [6,18,19]. AP-SALD has already been successfully utilized for the growth of uniform films for different applications including solar cells [20,21], light emitting diodes [22–24], and quantum tunneling diodes [25]. Here, we report on the first results of growing a 2D material on a dielectric film deposited by AP-SALD. Monolayer MoS₂ is grown via CVD on thin Al₂O₃ films deposited by AP-SALD.

By a detailed analysis we show that the combination of those two scalable approaches may be used to fabricate mm-sized samples largely covered with nano-crystalline *p*-doped 2D-MoS₂.

2. Results and Discussion

The growth of TMDCs via CVD is typically dominated by the material supply. This in turn is governed by the material sources, the TMDC itself, and the substrate. The most common substrate is thermally grown SiO₂ on top of a Si wafer, which allows the fabrication of field-effect transistors (FET) based on the as grown-material without an additional transfer step. This may however not be an ideal substrate for the synthesis of large MoS₂ samples, as thermally grown SiO₂ is amorphous and exhibits a typical roughness (root mean square) of $z_{RMS} = 0.5$ nm. Thus, if the fabrication on a FET is not the final goal, better suited substrates can be used which may facilitate large-scale growth. For MoS₂, epi-polished, single crystals of Al₂O₃ have proven to be an almost ideal substrate with atomic scale roughness and a lattice constant of $a_{Al_2O_3} = 4.8$ Å. The lattice is commensurable to the MoS₂ lattice ($a_{MoS_2} = 3.2$ Å [26]) and mm-sized, epitaxial monolayers could be grown via CVD [27]. As reference systems for our study, we have therefore grown MoS₂ via CVD on amorphous SiO₂ (see Fig. 1a) and on crystalline Al₂O₃ (see Fig. 1b; for details see method section). On both substrates, individual flakes with the typical star-like triangular form have grown. On average the flakes on SiO₂ are somewhat smaller than the ones on Al₂O₃. Both samples exhibit the typical in- and out-of-plane Raman modes E_{2g}¹ and A_{1g} at wavenumbers 382 cm⁻¹ and 403 cm⁻¹ for the SiO₂ substrate, and 385 cm⁻¹ and 402 cm⁻¹ for the sapphire substrate, respectively, as well as a strong photoluminescence signal at an energy around $E = 1.8$ eV, the latter confirming the materials' 2D nature. From the position of the Raman modes we deduced the strain and doping of the grown flakes following the approaches presented in Refs. [28–30]. We find that MoS₂ on SiO₂ exhibits a tensile strain of 0.45% and is highly n-doped with $n_e = 1.0 \times 10^{13}$ cm⁻², and on sapphire it shows a compressive strain of -0.3% and is similarly n-doped with $n_e = 1.2 \times 10^{13}$ cm⁻².

From Fig. 1 it is obvious that in principle the amorphous structure of SiO₂ does not prevent the synthesis of large monolayer flakes and thus it seems promising to investigate the possibility to grow TMDCs on amorphous Al₂O₃. To this end, a Si wafer with a 385 nm SiO₂ layer on top was used as a base substrate. Then, 20 nm of Al₂O₃ were deposited on top of the wafer via AP-SALD (for details, see method section), resulting in a seemingly continuous layer as shown in Fig. 2a. The thickness can be chosen freely within the limits of the method and in particular it can be chosen to be sufficiently thin to enable flexible devices. For the purpose of this study we have chosen 20 nm which should be thick enough to prevent the underlying SiO₂ layer from influencing the MoS₂ growth, e.g. by interface charges [30]. The Al₂O₃ layers deposited in this way have an average roughness of $z_{RMS} = 0.33$ nm, which is slightly larger than for a layer grown by conventional ALD ($z_{RMS} = 0.22$ nm, shown for

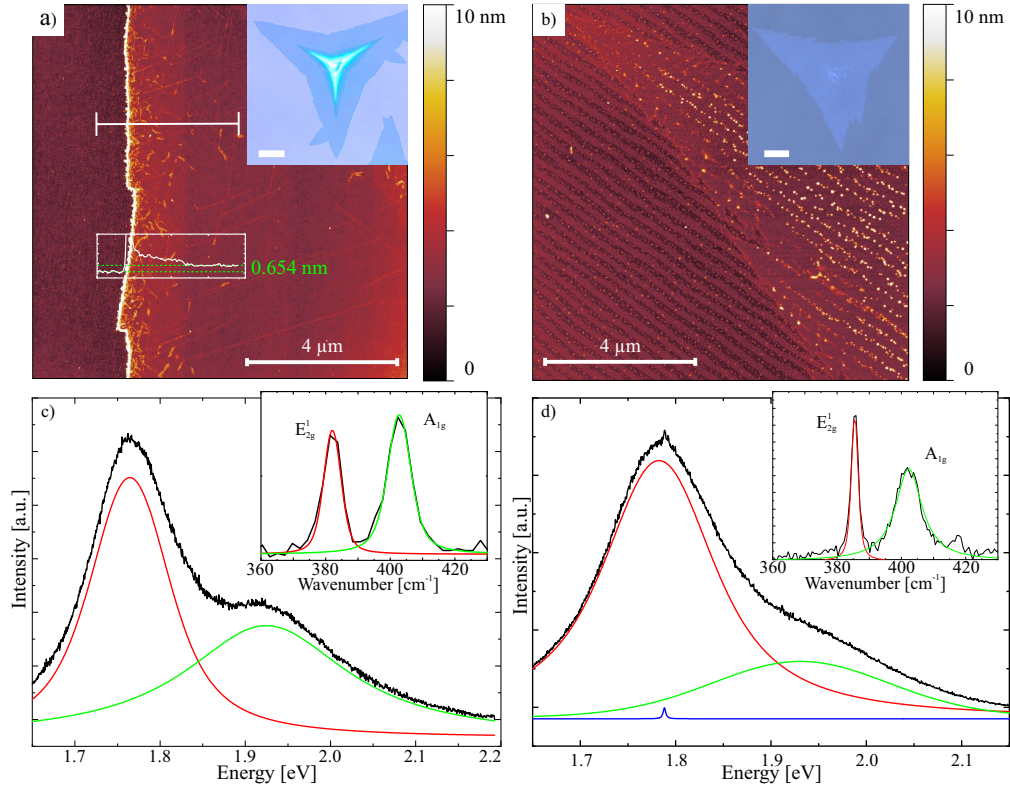


Figure 1. AFM/optical images and PL/Raman spectra of MoS₂ monolayers grown via CVD on the two most common substrates. AFM of MoS₂ on SiO₂ (a) and on sapphire (b), and the corresponding optical images (inset). The scale bar is 10 μm. The height of the layer was measured to be 0.654 nm (a, line, white), which is consistent with the nominal single layer height of MoS₂. (b) clearly shows the atomic terraces of the single crystalline substrate. The PL spectra from both samples show a distinct RT photoluminescence at 1.76 eV (SiO₂) and 1.8 eV (Al₂O₃), respectively, that is characteristic for the MoS₂ monolayer. The Raman spectra show the fingerprint A_{1g} and E_{2g}¹ vibrational modes.

comparison in Fig. 2b), but comparable to the roughness of a clean, amorphous SiO₂ surface.

The AP-SALD substrate was then used in a standard CVD process to deposit MoS₂ (for details, see method section). In Fig. 3a an optical image from the as-grown MoS₂ is shown. At the top left side of the sample, close to the material source, the MoS₂ has grown as individual flakes that have the typical triangular shape with a size of up to 100 μm. Moving to the bottom right, i.e., further downstream, one can see that the density of the flakes increases while their size decreases. This clearly shows that the amorphous AP-SALD substrate allows for very different flake morphologies, depending on the temperature and material supply. In particular, there is a large region, extending roughly from the middle of the first third of the substrate (position of the green square) to its lower left right edge, where the flake size appears to be too small to be resolved by optical microscopy and a seemingly

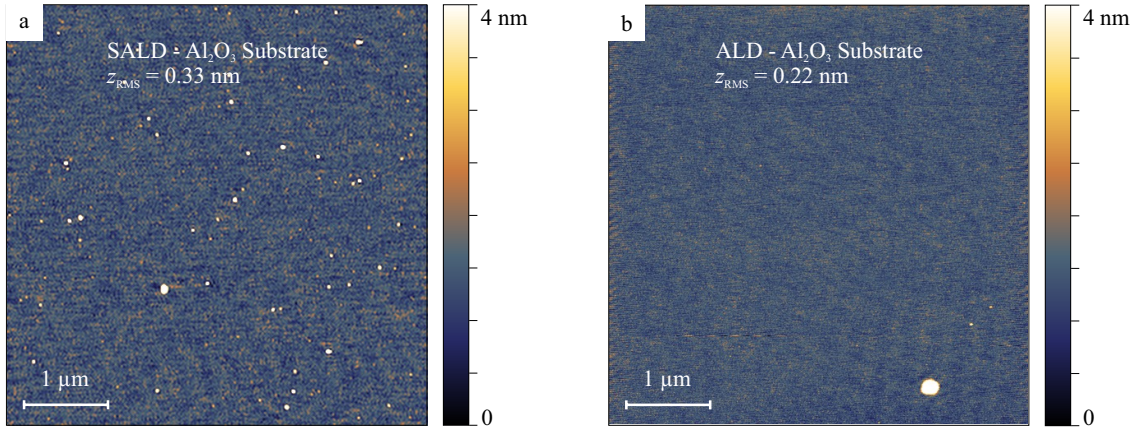


Figure 2. AFM images of the Al₂O₃ substrate deposited by AP-SALD (a), conventional ALD (b). In both cases a uniform, continuous layer is formed. The statistical analysis of the height data yields a roughness of about $z_{RMS} = 0.33$ nm for the AP-SALD layer and $z_{RMS} = 0.22$ nm for the ALD layer.

continuous film has been synthesized. Note, that this region is on the order of several square millimetres. To the best of our knowledge, this has never been achieved with an amorphous SiO₂/Si substrate and furthermore did also not occur on ALD-grown Al₂O₃ substrates (see SI). Further analysis with AFM reveals the true morphology in this region. As shown in Fig. 4, the seemingly uniform film is made up from densely packed nano-crystallites with an average height of $\simeq 7$ Å. The edge length of the individual flakes decreases from several microns (Fig. 4 a-c) down to <100 nm (Fig. 4 d-f) within a span of $120 \mu\text{m}$. At the same time the filling factor increases from 35% for the individual flakes to about 75% for the nano-crystallites.

To further verify that this nano-crystalline film region is made up from MoS₂ monolayer flakes, Raman and PL spectroscopies were performed. For easy comparison, we chose the transition region (green square in Fig. 3) and start upstream with an analysis of the individual flakes (Fig. 3b, black circle), where the Raman E_{2g}¹ and A_{1g} modes are found at 383 cm^{-1} and 404 cm^{-1} , i.e., exhibiting a difference of 21 cm^{-1} (Fig. 3c, black curve in the inset). The difference in wave numbers confirms that these flakes are single layer MoS₂ [31], and this is corroborated by a moderate PL at 1.8 eV (Fig. 3c, black curve). The PL signal shows a strong trion contribution at $\simeq 2.0 \text{ eV}$, as shown by the blue fits in Fig. 3c, that points towards a significant density of excess charges. From the Raman mode positions we again infer that the MoS₂ here is single layer [31], n-doped with $n_e = 0.2 \times 10^{13} \text{ cm}^{-2}$, and experiences a tensile strain of 0.3% [28–30]. The strain is comparable to that observed on the SiO₂ substrate (see Fig. 1), but the doping is reduced quite drastically when compared to both SiO₂ and sapphire as substrates.

Next, we will analyze the nano-crystalline region located further downstream (Fig. 3b,

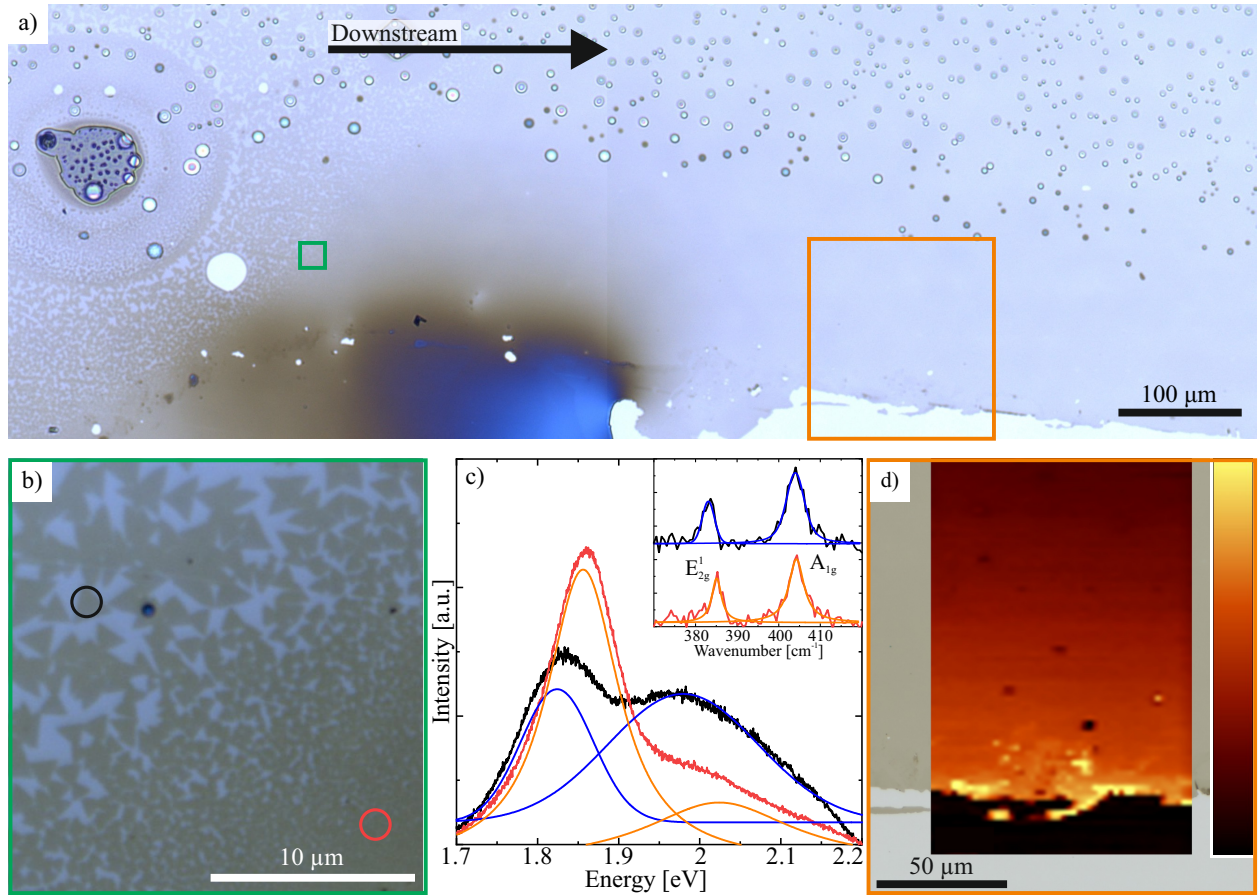


Figure 3. Optical images, exemplary Raman, PL spectra and mapping of MoS₂ monolayers grown via CVD on the AP-SALD-grown Al₂O₃ layer. Optical image (a) of the substrate fabricated by AP-SALD after the MoS₂ process. Downstream direction is marked with arrow. Separated flakes (upstream) are visible as well as a continuous layer of flakes (downstream). The transition area in between (green square) is shown in (b). The individual flakes have a triangular structure; Raman and PL spectra shown in (c) are taken from the areas marked by the circles. The PL peaks for the nano-crystallites (b, red) have more intensity and are more narrow than for the individual flakes (b, black). The Raman spectra show the typical MoS₂ modes for both (c, inset). The E_{2g}¹ and A_{1g} modes were measured at 383 cm⁻¹ and 404 cm⁻¹ for the individual flakes and at 385 cm⁻¹ and 404 cm⁻¹ for the nano-crystallites. A PL mapping (d) shows the intensity at 1.86 eV and that the nano-crystalline region expands over several hundred microns. In the lower part, where no PL activity is measured, no a-Al₂O₃ was deposited and no MoS₂ growth was detected.

red circle). Note, that the overall intensity of the MoS₂ Raman modes (Fig 3c, inset) is in general very low, compared to the Si signal at 520 cm⁻¹, which is probably due to the different optical properties of the AP-SALD substrate [32]. The different intensity ratio of the in-plane E_{2g}¹ mode and the A_{1g} mode maybe due to the different polarization dependence of the two modes [31].

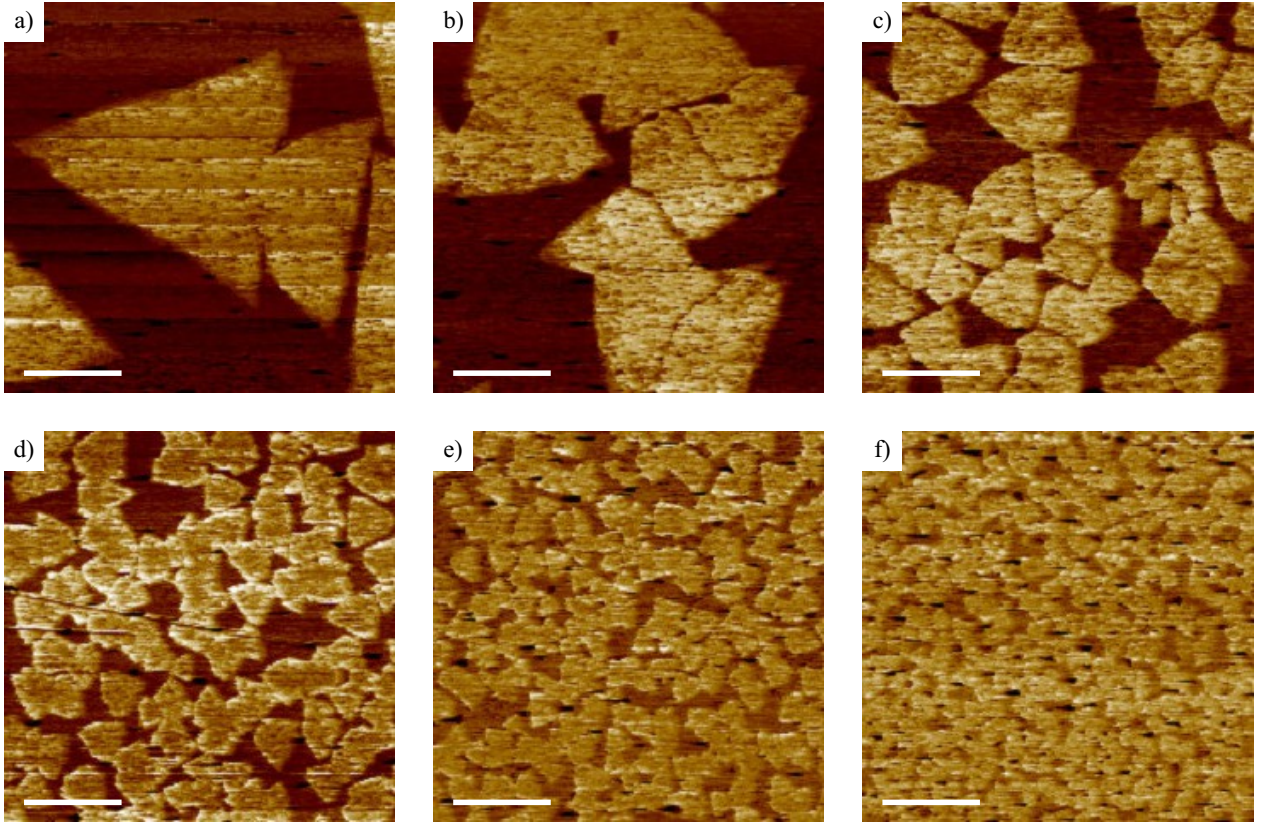


Figure 4. Peak-force-microscopy images taken in different regions of the sample starting from micron-sized individual flakes (a-c) in the upstream region to the nano-crystallites typically found in the downstream region (d-f). The filling factor increases from 49 % (a) to 73 % (f). The scale bar is 1 μm .

Despite the comparatively poor signal-to-noise ratio we were able to perform a quantitative analysis. We find that both in- and out-of-plane mode have shifted in comparison to the modes observed from individual flakes (see red and black curves in the inset of Fig. 3c), exhibiting an even smaller difference of 20 cm^{-1} . The E_{2g}^1 mode shifts to 385 cm^{-1} which shows that the strain of the material is now negligible with $<0.02\%$ and thus comparable to the reference value of freestanding MoS₂ [29, 33]. This relaxation is probably connected to the reduced size of the flakes. The A_{1g} mode red-shifts to 405 cm^{-1} and therefore the material here is *p*-doped with $n_h = 0.1 \times 10^{13} \text{ cm}^{-2}$ [29, 34]. The observed change in doping is in striking contrast to values reported in literature so far, where MoS₂ usually shows *n*-type doping on Al₂O₃ and SiO₂ [29, 35, 36], while *p*-type doping has been observed so far only on metallic substrates, as for example, Au [29, 37]. *P*-type doping of MoS₂ can be achieved in different ways [34, 38], e.g., also by adding appropriate reactants in the CVD process but the resulting carrier density determined in a field-effect transistor was an order of magnitude lower [39].

Interestingly, in comparison, the PL in the nano-crystalline region has a significantly higher intensity at an energy of about 1.85 eV (Fig. 3c, red curve). This considerable PL signal again confirms that the nano-crystallites consist of single layer MoS₂ [9]. The trion contribution is strongly reduced to $I_T/I_E = 0.78$ ($I_T/I_E = 0.54$ at 77 K, see SI) as derived from the orange fits in Fig. 3c. In comparison, the large flakes exhibit a ratio of $I_T/I_E = 2.00$. The reduced trion contribution indicates that less excess charge carriers are available and mirrors the red-shift of the Raman modes associated with p-type doping in the nano-crystalline region. Low-temperature PL measurements (see SI) show that the peaks barely shift (around 20 meV) which is to be expected for a non-strained monolayer. Finally, a PL mapping of a large sample region (Fig. 3d) shows that indeed the whole nano-crystalline film is PL-active.

3. Conclusion

We have synthesized monolayers of MoS₂ via CVD on thin films of Al₂O₃ grown via AP-SALD. The resulting flakes show a large variation in properties depending on their position on the substrate. While this effect is in principle well-known from all CVD processes [40], we observe a strong and quite unusual difference in morphology, and related to this, unexpected changes of vibrational and optoelectronic properties. In particular, while the larger, individual flakes show only weak, trion-dominated PL and appear n-doped and strained, we identified a region with a very high (up to 73 %) coverage of nano-crystalline MoS₂ with negligible strain, p-type doping and a significant PL emission dominated by the A exciton. Whether this unusual doping can be maintained upon further processing remains to be seen. The unique morphology of MoS₂ monolayer nano-crystallites with a high density of edges combined with a high coverage appears exclusively on the AP-SALD-grown substrates and could be advantageous for, e.g., catalysis [41], sensing [42] or electrochemical [43] applications. In terms of (flexible) devices, it would be beneficial to further increase the coverage up to a completely continuous, closed film. One way to achieve this could be a second processing step, exploiting the fact that the growth is dominated by the transport of material across the flake area (and not along the edges) [44], which could lead to a preferential growth in-between the pre-existing flakes. An alternative way could be to combine the AP-SALD-grown substrate with another variant of CVD, i.e, metal organic CVD which is known to produce uniform and closed layers of MoS₂ composed of many small crystallites [45].

4. Methods

4.1. Spatial Atomic Layer Deposition

AP-SALD is a modification of the conventional ALD approach, in which different precursor exposure steps of conventional ALD are not temporally but spatially separated. In this work, a custom-built, linear “zone-separated” AP-SALD system was used. This arrangement works with a fixed reactor head through which the individual precursor gases pass in different channels. The gases exit in parallel streams at different locations on the bottom of the head creating precursor filled zones. The individual zones are separated by an inert nitrogen gas. Furthermore, in between the individual gas channels, there are exhaust channels through which the gases are removed using a vacuum pump. The substrate was placed on a heated substrate stage approximately 100 μm below the reactor head and oscillated back and forth at 50 mm/s to deposit a film with the desired 20 nm thickness (80 cycles). By eliminating the vacuum chamber and purge steps, the throughput is higher and the process more cost effective than that of a conventional ALD system.

Trimethylaluminum (TMA, Strem Chemicals) and distilled water were used as the precursors. To deliver the TMA to the reactor head, nitrogen was bubbled through the TMA at 38 sccm and combined with a carrier nitrogen flow of 87 sccm. Similarly, the distilled water was bubbled with a 125 sccm nitrogen flow and combined with a carrier nitrogen flow of 125 sccm. A flow of 2000 sccm was delivered to 6 inert nitrogen gas channels separating the precursor channels. The heated substrate stage was held at 250 °C throughout the deposition.

4.2. Atomic Layer Deposition

In this process, three precursors were employed: Trimethylaluminum (TMA), O₂ plasma and Argon (Ar) as inert gas. 50 cycles were used to deposit 5 nm thick Al₂O₃ film. The film was deposited at 100 °C with a pressure of 1.3×10^{-4} Pa. The reactor chamber was first purged with Ar for 3 min to stabilize the chamber temperature and pressure. Ar was bubbled through TMA to dose the substrate for 20 ms at a pressure of 2 Pa, and then the precursor line was purged with Ar for 1 s at a pressure of 2 Pa. After that, a flow of O₂ was stabilized for 500 ms before generating a plasma by RF with a power of 300 W at a pressure of 2 Pa. The substrate was then exposed to the O₂ plasma for 2 s and followed by purging for 1 s.

4.3. Chemical Vapor Deposition

The custom-made synthesis protocol is based on the system by Lee et al. [46] and is used to fabricate crystalline MoS₂ monolayers on various substrates [28]. The SiO₂ substrate was a *p*-doped silicon wafer in (100) orientation with a 285 nm oxide thickness from *Graphene Supermarket*. The Sapphire substrate was a *c*-plane (0001), epi-polished monocrystalline

Al₂O₃ wafer with a 0.2° offcut from *Roditi*. It was annealed at 1000 °C for 60 min prior to synthesis.

The molybdenum source was ammonium heptamolybdate (AHM, Sigma Aldrich), an inorganic ammonium salt soluble in water. The solution with 200 g L⁻¹ was deposited onto the substrate in a single droplet of 1 mm in diameter at the upstream edge of the substrate. This substrate including the precursor material was heated to 300 °C for 30 min to form MoO₃ [47]. In a 1 Vol% solution the seeding promoter, cholic acid sodium salt (Sigma Aldrich), was spin coated onto the substrate containing the MoO₃ and put into a crucible. A second crucible was filled with 40 mg sulfur (S powder, Sigma Aldrich, 99.98 %). The chemical vapor deposition took place in a tube furnace (ThermConcept, ROK 70/750/12-3z) with three thermally separated heating zones. The crucible containing the substrates was placed into the second heating zone (downstream) and the crucible containing the sulfur was placed into the first heating zone (upstream). The tube was purged with inert argon gas. For the synthesis, the Ar flow rate was set to 500 sccm. The downstream zone was heated to 750 °C in 10 min and held at that temperature for 20 min. The upstream zone is heated to 150 °C in 10 min and held at that temperature for 20 min. The process is ended by rapidly cooling down the samples.

4.4. Atomic force microscopy

Atomic force microscopy images were taken with a *Veeco Dimension 3100 AFM* in tapping-mode using Nanosensors NCHR-50 tips. The peak-force-microscopy measurements were performed with a *Bruker Dimension Icon* in the PeakForce Tapping Mode using ScanAsyst-Air tips. The AFM results were analyzed and visualized by *Gwyddion 2.60*. The filling factors were evaluated by increasing the contrast between flakes and substrate until a black and white image was obtained and the counting the respective pixels.

4.5. Raman and Photoluminescence spectroscopy

Raman and PL spectroscopy were performed with a *WiTec alpha300 RA* confocal Raman spectrometer. All measurements were performed with 532 nm excitation wavelength and an output power of 4 mW. For Raman measurements a 1800 cm⁻¹ grid, and for PL measurements a 300 cm⁻¹ grid was used, respectively.

Acknowledgment

We thank ICAN (S. Franzka) for conducting the peak-force-microscopy measurements and acknowledge financial support from the Federal Ministry of Education and Research (BMBF, project 05K19PG1), the German Research Foundation (DFG, SCHL 384/20-1, project number 406129719) and from CENIDE. K.P.M. acknowledges funding from NSERC

Discovery (RGPIN-2017-04212, RGPAS-2017-507977), Canada Foundation For Innovation John R. Evans Leaders Fund (Project 35552), and Ontario Ministry of Research, Innovation and Science ORF-Small Infrastructure (Project 35552). The University of Waterloo's QNFCF facility was used for this work.

- [1] C. Chen, Z. Feng, Y. Feng, Y. Yue, C. Qin, D. Zhang, and W. Feng, "Large-scale synthesis of a uniform film of bilayer MoS₂ on graphene for 2d heterostructure phototransistors," *ACS Applied Materials & Interfaces*, vol. 8, no. 29, pp. 19004–19011, 2016.
- [2] W. J. Yu, Y. Liu, H. Zhou, A. Yin, Z. Li, Y. Huang, and X. Duan, "Highly efficient gate-tunable photocurrent generation in vertical heterostructures of layered materials," *Nature Nanotechnology*, vol. 8, no. 12, pp. 952–958, 2013.
- [3] W. Zhang, C.-P. Chuu, J.-K. Huang, C.-H. Chen, M.-L. Tsai, Y.-H. Chang, C.-T. Liang, Y.-Z. Chen, Y.-L. Chueh, J.-H. He, M.-Y. Chou, and L.-J. Li, "Ultrahigh-gain photodetectors based on atomically thin graphene-MoS₂ heterostructures," *Scientific reports*, vol. 4, p. 3826, 2014.
- [4] L. Yu, Y.-H. Lee, X. Ling, E. J. G. Santos, Y. C. Shin, Y. Lin, M. Dubey, E. Kaxiras, J. Kong, H. Wang, and T. Palacios, "Graphene/MoS₂ hybrid technology for large-scale two-dimensional electronics," *Nano Letters*, vol. 14, no. 6, pp. 3055–3063, 2014.
- [5] M. Amani, R. A. Burke, R. M. Proie, and M. Dubey, "Flexible integrated circuits and multifunctional electronics based on single atomic layers of MoS₂ and graphene," *Nanotechnology*, vol. 26, no. 11, p. 115202, 2015.
- [6] K. P. Musselman, C. F. Uzoma, and M. S. Miller, "Nanomanufacturing: High-throughput, cost-effective deposition of atomic scale thin films via atmospheric pressure spatial atomic layer deposition," *Chemistry of Materials*, vol. 28, no. 23, pp. 8443–8452, 2016.
- [7] H. Bergeron, V. K. Sangwan, J. J. McMorro, G. P. Campbell, I. Balla, X. Liu, M. J. Bedzyk, T. J. Marks, and M. C. Hersam, "Chemical vapor deposition of monolayer MoS₂ directly on ultrathin Al₂O₃ for low-power electronics," *Applied Physics Letters*, vol. 110, no. 5, p. 053101, 2017.
- [8] K. F. Mak, C. Lee, J. Hone, J. Shan, and T. F. Heinz, "Atomically thin MoS₂: a new direct-gap semiconductor," *Science*, vol. 105, no. 13, p. 136805, 2010.
- [9] A. Kuc, N. Zibouche, and T. Heine, "Influence of quantum confinement on the electronic structure of the transition metal sulfide TS₂," *Physical Review B*, vol. 83, no. 24, p. 4059, 2011.
- [10] A. Splendiani, L. Sun, Y. Zhang, T. Li, J. Kim, C.-Y. Chim, G. Galli, and F. Wang, "Emerging photoluminescence in monolayer MoS₂," *Nano Letters*, vol. 10, no. 4, pp. 1271–1275, 2010.
- [11] E. Pollmann, J. M. Morbec, L. Madau, L. Bröckers, P. Kratzer, and M. Y. Schleberger, "Molybdenum disulphide nanoflakes grown by chemical vapour deposition on graphite: Nucleation, orientation, and charge transfer," *The Journal of Physical Chemistry C*, 2020.
- [12] E. Pollmann, L. Madau, S. Schumacher, U. Kumar, F. Heuvel, C. vom Ende, S. Yilmaz, S. Güngörmüs, and M. Schleberger, "Apparent differences between single layer molybdenum disulphide fabricated via chemical vapour deposition and exfoliation," *Nanotechnology*, vol. 31, no. 50, p. 505604, 2020.
- [13] J. Zhou, J. Lin, X. Huang, Y. Zhou, Y. Chen, J. Xia, H. Wang, Y. Xie, H. Yu, J. Lei, Di Wu, F. Liu, Q. Fu, Q. Zeng, C.-H. Hsu, C. Yang, L. Lu, T. Yu, Z. Shen, H. Lin, B. I. Yakobson, Q. Liu, K. Suenaga, G. Liu, and Z. Liu, "A library of atomically thin metal chalcogenides," *Nature*, vol. 556, no. 7701, pp. 355–359, 2018.
- [14] H. Kattelus, M. Ylilammi, J. Saarilahti, J. Antson, and S. Lindfors, "Layered tantalum-aluminum oxide films deposited by atomic layer epitaxy," *Thin Solid Films*, vol. 225, no. 1-2, pp. 296–298, 1993.
- [15] K. Kukli, "Properties of Ta₂O₅-based dielectric nanolaminates deposited by atomic layer epitaxy," *Journal of The Electrochemical Society*, vol. 144, no. 1, p. 300, 1997.
- [16] K. Kukli, J. Ihanus, M. Ritala, and M. Leskela, "Tailoring the dielectric properties of HfO₂ – Ta₂O₅ nanolaminates," *Applied Physics Letters*, vol. 68, no. 26, pp. 3737–3739, 1996.
- [17] J. A. Liddle and G. M. Gallatin, "Nanomanufacturing: A perspective," *ACS Nano*, vol. 10, no. 3, pp. 2995–3014, 2016.
- [18] K. Mistry, A. Jones, M. Kao, T. W.-K. Yeow, M. Yavuz, and K. P. Musselman, "In-situ observation of nucleation and property evolution in films grown with an atmospheric pressure spatial atomic layer deposition system," *Nano Express*, vol. 1, no. 1, p. 010045, 2020.

- [19] P. Poodt, A. Lankhorst, F. Roozeboom, K. Spee, D. Maas, and A. Vermeer, "High-speed spatial atomic-layer deposition of aluminum oxide layers for solar cell passivation," *Advanced Materials (Deerfield Beach, Fla.)*, vol. 22, no. 32, pp. 3564–3567, 2010.
- [20] K. P. Musselman, S. Albert-Seifried, R. L. Z. Hoye, A. Sadhanala, D. Muñoz-Rojas, J. L. MacManus-Driscoll, and R. H. Friend, "Improved exciton dissociation at semiconducting polymer: ZnO donor:acceptor interfaces via nitrogen doping of ZnO," *Advanced Functional Materials*, vol. 24, no. 23, pp. 3562–3570, 2014.
- [21] Y. Ievskaya, R. L. Z. Hoye, A. Sadhanala, K. P. Musselman, and J. L. MacManus-Driscoll, "Improved heterojunction quality in Cu₂O-based solar cells through the optimization of atmospheric pressure spatial atomic layer deposited zn1-xmgxo," *Journal of visualized experiments : JoVE*, no. 113, 2016.
- [22] R. L. Z. Hoye, K. P. Musselman, M. R. Chua, A. Sadhanala, R. D. Raninga, J. L. MacManus-Driscoll, R. H. Friend, and D. Credgington, "Bright and efficient blue polymer light emitting diodes with reduced operating voltages processed entirely at low-temperature," *Journal of Materials Chemistry C*, vol. 3, no. 36, pp. 9327–9336, 2015.
- [23] R. L. Z. Hoye, M. R. Chua, K. P. Musselman, G. Li, M.-L. Lai, Z.-K. Tan, N. C. Greenham, J. L. MacManus-Driscoll, R. H. Friend, and D. Credgington, "Enhanced performance in fluorene-free organometal halide perovskite light-emitting diodes using tunable, low electron affinity oxide electron injectors," *Advanced Materials (Deerfield Beach, Fla.)*, vol. 27, no. 8, pp. 1414–1419, 2015.
- [24] D. Di, Le Yang, J. M. Richter, L. Meraldi, R. M. Altamimi, A. Y. Alyamani, D. Credgington, K. P. Musselman, J. L. MacManus-Driscoll, and R. H. Friend, "Efficient triplet exciton fusion in molecularly doped polymer light-emitting diodes," *Advanced Materials (Deerfield Beach, Fla.)*, vol. 29, no. 13, 2017.
- [25] A. H. Alshehri, K. Mistry, V. H. Nguyen, K. H. Ibrahim, D. Muñoz-Rojas, M. Yavuz, and K. P. Musselman, "Quantum-tunneling metal-insulator-metal diodes made by rapid atmospheric pressure chemical vapor deposition," *Advanced Functional Materials*, vol. 29, no. 7, p. 1805533, 2019.
- [26] N. Wakabayashi, H. G. Smith, and R. M. Nicklow, "Lattice dynamics of hexagonal MoS₂ studied by neutron scattering," *Physical Review B*, no. 12(2), pp. 659–663, 1975.
- [27] D. Duncenco, D. Ovchinnikov, K. Marinov, P. Lazić, M. Gibertini, N. Marzari, O. Lopez Sanchez, Y.-C. Kung, D. Krasnozhan, M.-W. Chen, S. Bertolazzi, P. Gillet, A. Fontcuberta i Morral, A. Radenovic, and A. Kis, "Large-area epitaxial monolayer MoS₂," *ACS Nano*, vol. 9, no. 4, pp. 4611–4620, 2015.
- [28] E. Pollmann, L. Madauß, V. Zeuner, and M. Schleberger, "Strain in single-layer MoS₂ flakes grown by chemical vapor deposition," in *Encyclopedia of Interfacial Chemistry*, pp. 338–343, Elsevier, 2018.
- [29] S. E. Panasci, E. Schilirò, G. Greco, M. Cannas, F. M. Gelardi, S. Agnello, F. Roccaforte, and F. Giannazzo, "Strain, doping, and electronic transport of large area monolayer MoS₂ exfoliated on gold and transferred to an insulating substrate," *ACS Applied Materials & Interfaces*, vol. 13, no. 26, pp. 31248–31259, 2021.
- [30] E. Schilirò, R. Lo Nigro, S. E. Panasci, S. Agnello, M. Cannas, F. M. Gelardi, F. Roccaforte, and F. Giannazzo, "Direct atomic layer deposition of ultrathin aluminum oxide on monolayer MoS₂ exfoliated on gold: The role of the substrate," *Advanced Materials Interfaces*, vol. 8, no. 21, p. 2101117, 2021.
- [31] C. Lee, H. Yan, L. E. Brus, T. F. Heinz, J. Hone, and S. Ryu, "Anomalous lattice vibrations of single- and few-layer MoS₂," *ACS Nano*, vol. 4, no. 5, pp. 2695–2700, 2010.
- [32] H. Zhang, Y. Wan, Y. Ma, W. Wang, Y. Wang, and L. Dai, "Interference effect on optical signals of monolayer MoS₂," *Applied Physics Letters*, vol. 107, no. 10, p. 101904, 2015.
- [33] D. Lloyd, X. Liu, J. W. Christopher, L. Cantley, A. Wadehra, B. L. Kim, B. B. Goldberg, A. K. Swan, and J. S. Bunch, "Band gap engineering with ultralarge biaxial strains in suspended monolayer MoS₂," *Nano Letters*, vol. 16, no. 9, pp. 5836–5841, 2016.
- [34] E. Z. Xu, H. M. Liu, K. Park, Z. Li, Y. Losovyj, M. Starr, M. Werbianskyj, H. A. Fertig, and S. X. Zhang,

- “p-type transition-metal doping of large-area MoS₂ thin films grown by chemical vapor deposition,” *Nanoscale*, vol. 9, no. 10, pp. 3576–3584, 2017.
- [35] K. F. Mak, K. He, C. Lee, G. H. Lee, J. Hone, T. F. Heinz, and J. Shan, “Tightly bound trions in monolayer MoS₂,” *Nature Materials*, vol. 12, no. 3, pp. 207–211, 2013.
- [36] B. Radisavljevic, A. Radenovic, J. Brivio, V. Giacometti, and A. Kis, “Single-layer MoS₂ transistors,” *Nature Nanotechnology*, vol. 6, no. 3, pp. 147–150, 2011.
- [37] E. Pollmann, S. Sleziuna, T. Foller, U. Hagemann, C. Gorynski, O. Petri, L. Madau, L. Breuer, and M. Schleberger, “Large-area, two-dimensional MoS₂ exfoliated on gold: Direct experimental access to the metal-semiconductor interface,” *ACS omega*, vol. 6, no. 24, pp. 15929–15939, 2021.
- [38] X. Xin, Y. Song, S. Guo, Y. Zhang, B. Wang, Y. Wang, and X. Li, “One-step synthesis of p-doped MoS₂ for efficient photocatalytic hydrogen production,” *Journal of Alloys and Compounds*, vol. 829, p. 154635, 2020.
- [39] J. S. Lee, C.-S. Park, T. Y. Kim, Y. S. Kim, and E. K. Kim, “Characteristics of p-type conduction in p-doped MoS₂ by phosphorous pentoxide during chemical vapor deposition,” *Nanomaterials (Basel, Switzerland)*, vol. 9, no. 9, 2019.
- [40] N. Kumar, R. Tomar, N. Wadehra, M. M. Devi, B. Prakash, and S. Chakraverty, “Growth of highly crystalline and large scale monolayer MoS₂ by cvd: The role of substrate position,” *Crystal Research and Technology*, vol. 53, no. 6, p. 1800002, 2018.
- [41] L. Madau, I. Zegkinoglou, H. Vázquez Muiños, Y.-W. Choi, S. Kunze, M.-Q. Zhao, C. H. Naylor, P. Ernst, E. Pollmann, O. Ochedowski, H. Lebius, A. Benyagoub, B. Ban-d’Etat, A. T. C. Johnson, F. Djurabekova, B. Roldan Cuenya, and M. Schleberger, “Highly active single-layer MoS₂ catalysts synthesized by swift heavy ion irradiation,” *Nanoscale*, vol. 10, no. 48, pp. 22908–22916, 2018.
- [42] B. Cho, M. G. Hahm, M. Choi, J. Yoon, A. R. Kim, Y.-J. Lee, S.-G. Park, J.-D. Kwon, C. S. Kim, M. Song, Y. Jeong, K.-S. Nam, S. Lee, T. J. Yoo, C. G. Kang, B. H. Lee, H. C. Ko, P. M. Ajayan, and D.-H. Kim, “Charge-transfer-based gas sensing using atomic-layer MoS₂,” *Scientific reports*, vol. 5, p. 8052, 2015.
- [43] G. Li, Du Zhang, Q. Qiao, Y. Yu, D. Peterson, A. Zafar, R. Kumar, S. Curtarolo, F. Hunte, S. Shannon, Y. Zhu, W. Yang, and L. Cao, “All the catalytic active sites of MoS₂ for hydrogen evolution,” *Journal of the American Chemical Society*, vol. 138, no. 51, pp. 16632–16638, 2016.
- [44] E. Pollmann, A. Maas, D. Marnold, A. Hucht, R. Neubieser, M. Stief, L. Madau, and M. Schleberger, “Dynamic growth/etching model for the synthesis of two-dimensional transition metal dichalcogenides via chemical vapour deposition.”
- [45] K. Kang, S. Xie, L. Huang, Y. Han, P. Y. Huang, K. F. Mak, C.-J. Kim, D. Muller, and J. Park, “High-mobility three-atom-thick semiconducting films with wafer-scale homogeneity,” *Nature*, vol. 520, no. 7549, pp. 656–660, 2015.
- [46] Y.-H. Lee, X.-Q. Zhang, W. Zhang, M.-T. Chang, C.-T. Lin, K.-D. Chang, Y.-C. Yu, J. T.-W. Wang, C.-S. Chang, L.-J. Li, and T.-W. Lin, “Synthesis of large-area MoS₂ atomic layers with chemical vapor deposition,” *Advanced Materials (Deerfield Beach, Fla.)*, vol. 24, no. 17, pp. 2320–2325, 2012.
- [47] Z. M. Hanafi, M. A. Khilli, and M. H. Askar, “The thermal decomposition of ammonium heptamolybdate,” *Thermochimica Acta*, vol. 45, no. 3, pp. 221–232, 1981.